Electronic Supplementary Material (ESI) for Journal of Materials Chemistry A.
This journal is © The Royal Society of Chemistry 2018

Supplementary Information

A novel ball milling technique for room temperature processing of TiO_2 nanoparticles employed as electron transport layer in perovskite solar cells and modules

Mriganka Singh,[a] Chien-Hung Chiang,[b] Karunakara Moorthy Boopathi,[c] Chintam Hanmandlu[c], Gang Li,[e] Chun-Guey Wu,*[bf] Hong-Cheu Lin,*[a] and Chih-Wei Chu*[cdg]

[a] *Department of Materials Science and Engineering, National Chiao Tung University, Hsinchu, Taiwan. Email: linhc@cc.nctu.edu.tw*

[b] *Research Center for New Generation Photovoltaics, National Central University, Jhong-Li, Taiwan. Email: t610002@cc.ncu.edu.tw*

[c] *Research Center for Applied Sciences, Academia Sinica, Taipei, Taiwan. Email: gchu@gate.sinica.edu.tw*

[d] *College of Engineering, Chang Gung University, Guishan District, Taoyuan City, Taiwan*

[e] *Department of Electronic and Information Engineering, The Hong Kong Polytechnic University, Hung Hom, Kowloon, Hong Kong, China*

[f] *Department of Chemistry, National Central University, Jhong-Li, Taiwan*

[g] *Department of Materials Science and Engineering, National Tsing Hua University, Hsinchu, Taiwan*

Table S1: PV performance of PSCs on different types of TiO_2 ETLs at the reverse and forward scans, measured under AM 1.5G illumination (100 mW/cm^2).

Device Structure	Scan direction	V_{oc} (V)	J_{sc} (mA cm^{-2})	*FF* (-)	*PCE* (%)
S-TiO_2	Reverse	1.02	20.00	0.60	12.32
	Forward	0.91	19.85	0.56	10.20
S-TiO_2/m-TiO2	Reverse	1.10	21.48	0.77	18.21
	Forward	1.01	21.49	0.63	13.92
G-TiO_2	Reverse	1.07	21.72	0.75	17.43
	Forward	1.05	21.63	0.75	17.03

Table S2: The device performance of PSCs (small-area: ≤ 0.1 cm^2) based on low-temperature TiO_2 ETL prepared with various deposition methods.

No.	Device Structure (only ETL)	ETL deposition method	ETL processing temperature (°C)	V_{oc} (V)	J_{sc} (mA cm^{-2})	*FF* *(-)*	*PCE* (%)	Year/ Ref.
1	FTO/TiO_2	hydrothermal	150	1.00	17.7	0.61	10.0	2013/
	FTO/TiO_2 + graphene			1.04	21.9	0.73	15.6	[1]
2	ITO/ TiO_2	non-hydrolytic sol-gel	150	1.06	19.9	0.65	13.8	2014/
	ITO/PEIE/ Y:TiO_2			1.13	22.7	0.75	19.3	[2]
3	FTO/TiO_x	non-hydrolytic sol-gel	150	0.96	15.4	0.56	8.3	2014/
	FTO/lt-TiO_2			1.05	20.0	0.72	15.3	[3]
4	ITO/TiO_2	non-hydrolytic sol-gel	150	1.02	21.0	0.72	15.6	2016/
	ITO/TiCl-TiO_2			1.09	19.7	0.75	16.4	[4]
5	ITO/TiO_2	non-hydrolytic sol-gel	150	1.03	19.1	0.77	15.1	2017/
	ITO/CQDs /TiO_2			1.13	21.3	0.78	18.8	[5]
6	ITO/TiO_2	non-hydrolytic sol-gel	150	1.12	21.6	0.76	18.5	2017/
	ITO/TiO_2-Cl			1.18	22.3	0.80	21.4	[6]
7	ITO/G-TiO_2	ball milling	<150	1.07	21.7	0.75	17.4	[This work]

Table S3: The efficiency of the perovskite solar submodules with various area based on TiO_2 ETL prepared at various temperature.[7]

No.	Device Structure (only ETL)	ETL processing temperature (°C)	Aperture area (cm^2)	Active area (cm^2)	Designated area (cm^2)	*PCE* (%)	Ref.
1	C-TiO_2	130	4.00	–	–	13.6	[8]
2	C-TiO_2/M-TiO_2	450	–	49.0	–	10.4	[9]
3	C-TiO_2	450	–	11.09	–	13.3	[10]
4	C-TiO_2/M-TiO_2	500	–	31.0	–	10.46	[11]
			–	70.0	–	10.74	
5	C-TiO_2/Graphene + M- TiO_2	450	–	50.6	–	12.6	[12]
6	C-TiO_2/M-TiO_2	500	–	8.40	–	6.22	[13]
7	C-TiO_2/M-TiO_2	480	–	8.80	–	9.50	[14]
8	C-TiO_2/TiO_2 NRs	450	–	8.80	–	8.07	[15]
9	C-TiO_2/M-TiO_2	500	36.1	–	–	15.8	[16]
			17.6	–	–	13.9	
			36.1	–	–	12.1(certified)	
10	C-TiO_2/M-TiO_2	480	_	10.1	_	10.3	[17]
			_	100	_	4.30	
11	C-TiO_2	450	10.36	_	_	15.14	[18]
12	C-TiO_2	500	_	2.02	_	13.53	[19]
13	G-TiO_2	<150	–	43.2	25.2	14.19	This work

Note. C-TiO_2: Compact TiO_2 layer; M-TiO_2: Mesoporous TiO_2 layer; G-TiO_2: Ground TiO_2 layer

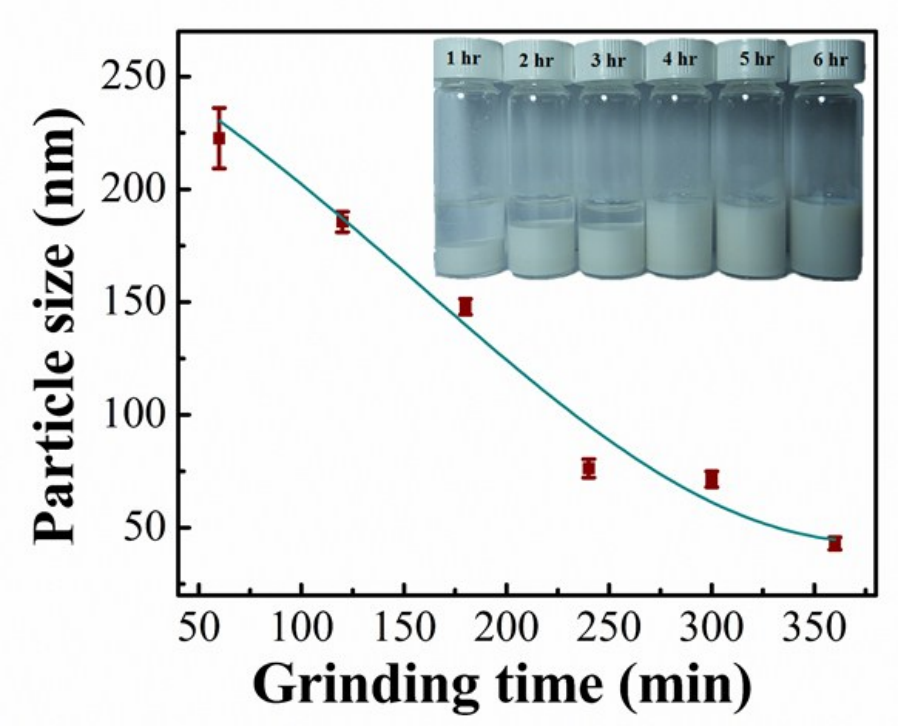

Fig. S1: Average particle size of TiO_2 powder plotted with respect to the grinding time (insert: the pictures of the ground TiO_2 solutions obtained different grinding times).

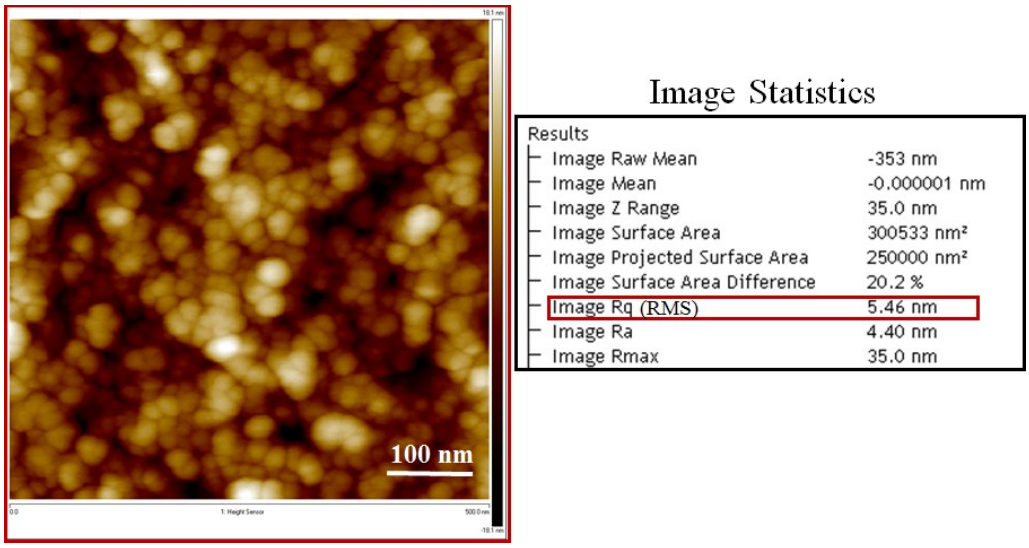

Fig. S2: Atomic force microscopy image of G-TiO_2 film spin-coated on ITO.

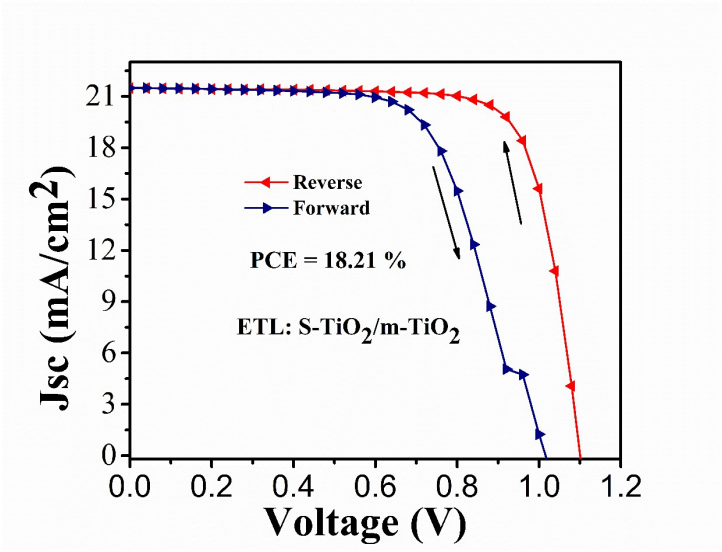

Fig. S3: *J-V* curve of PSCs with the device structure FTO/S-TiO_2/m-TiO_2/$CH_3NH_3PbI_3$/spiro-MeOTAD/MoO_3/Ag measured at reverse and forward scans.

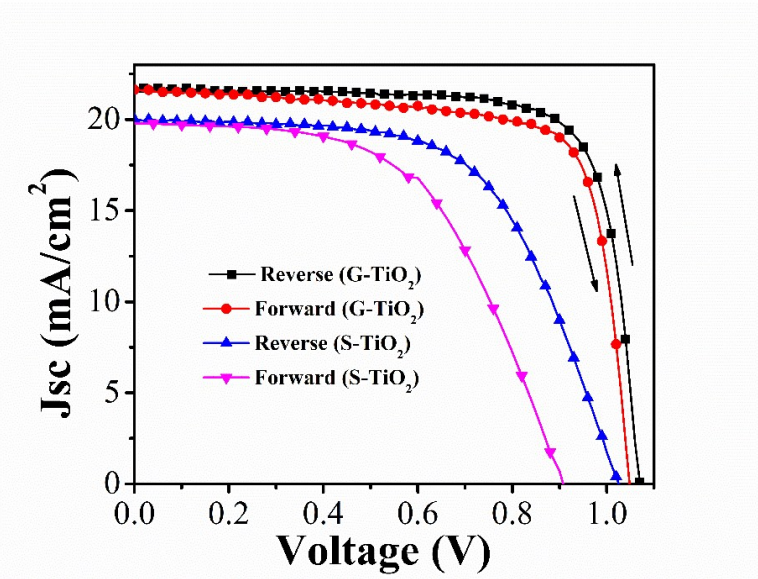

Fig. S4: *J-V* curves of PSCs with the G-TiO_2 and S-TiO_2 as an electron transporting layers measured at reverse and forward scans.

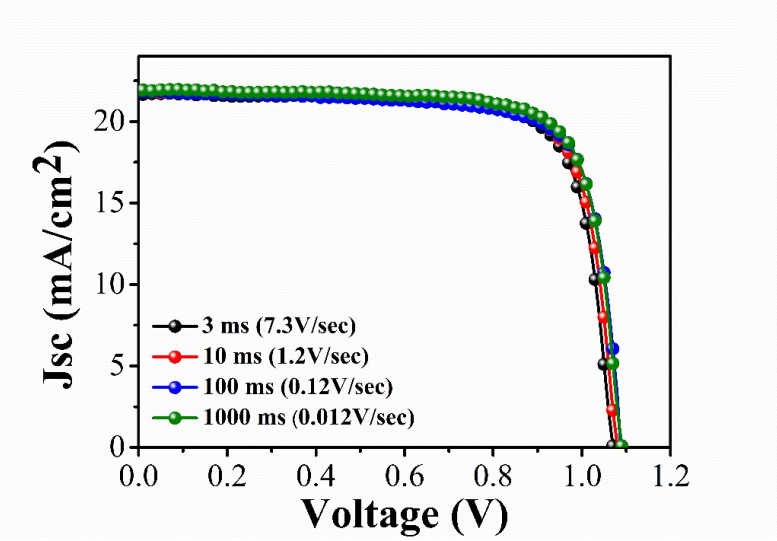

Fig. S5: *J-V* curves of of the G-TiO_2 based PSCs measured with different delay times.

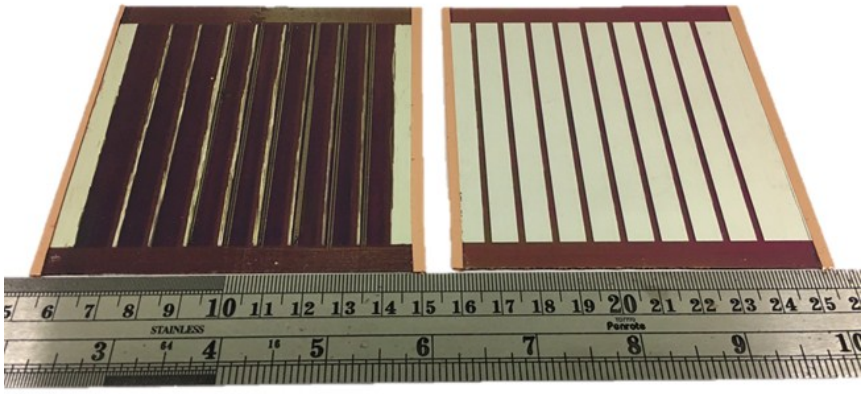

Fig. S6: Photograph of large-area (25.2 cm^2) solar submodules incorporating G-TiO_2 as the ETL.

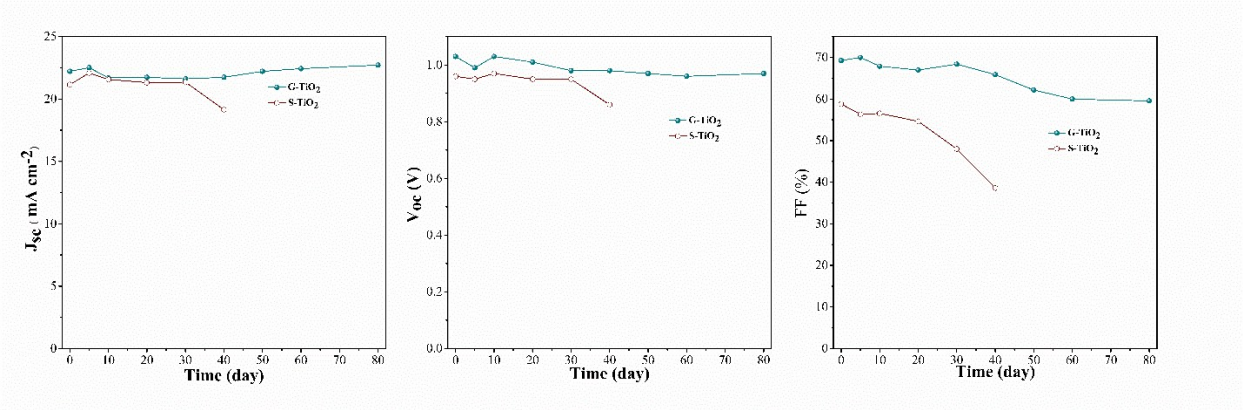

Fig. S7: Long-term stability tests of the best cell [ITO (or FTO)/G-TiO_2 (or S-TiO_2) /$CH_3NH_3PbI_3$/spiro-MeOTAD/MoO_3/Ag] stored in a glove box under N_2.

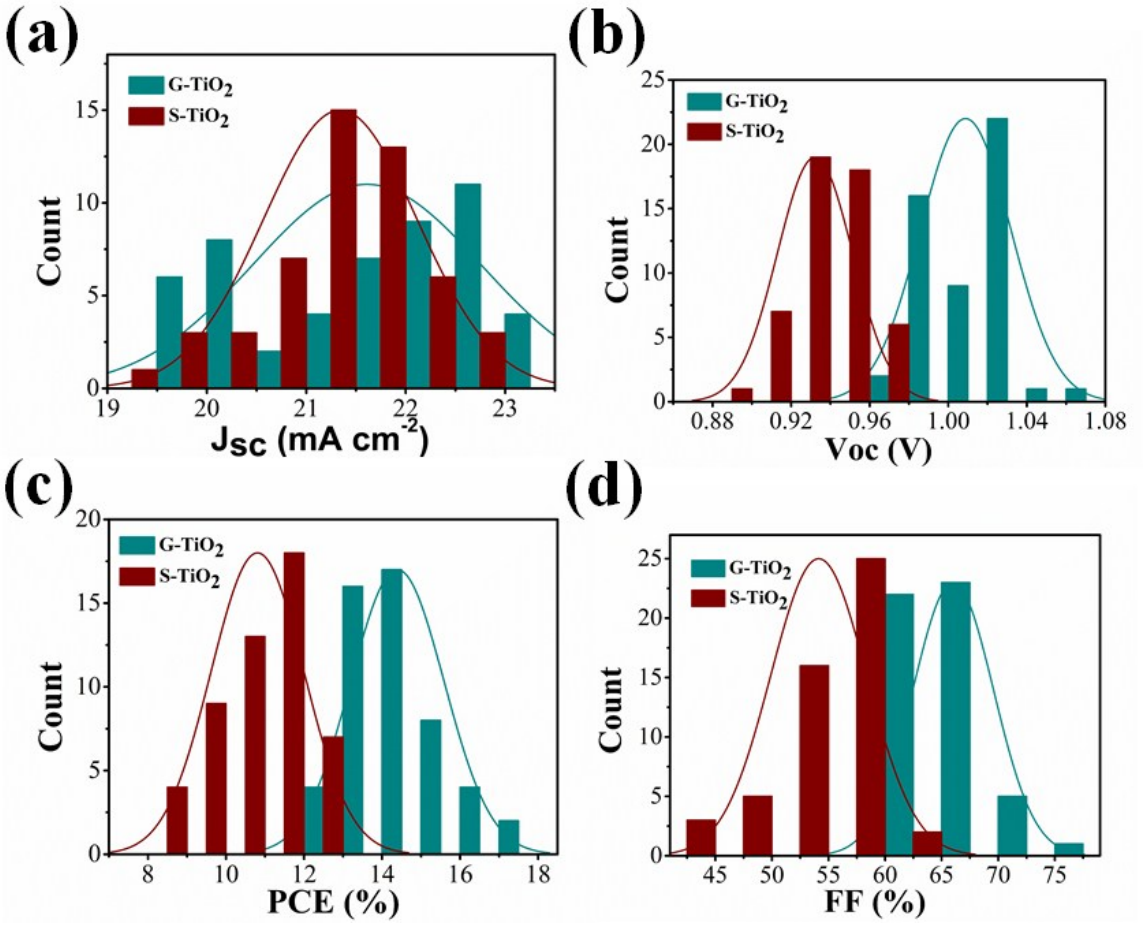

Fig. S8: Histograms of the performance (current-density, open-circuit voltage, power conversion efficiency, and fill factor) of 51 G-TiO_2 and S-TiO_2 devices, measured under 1 Sun light illumination (100 mW cm^{-2}).

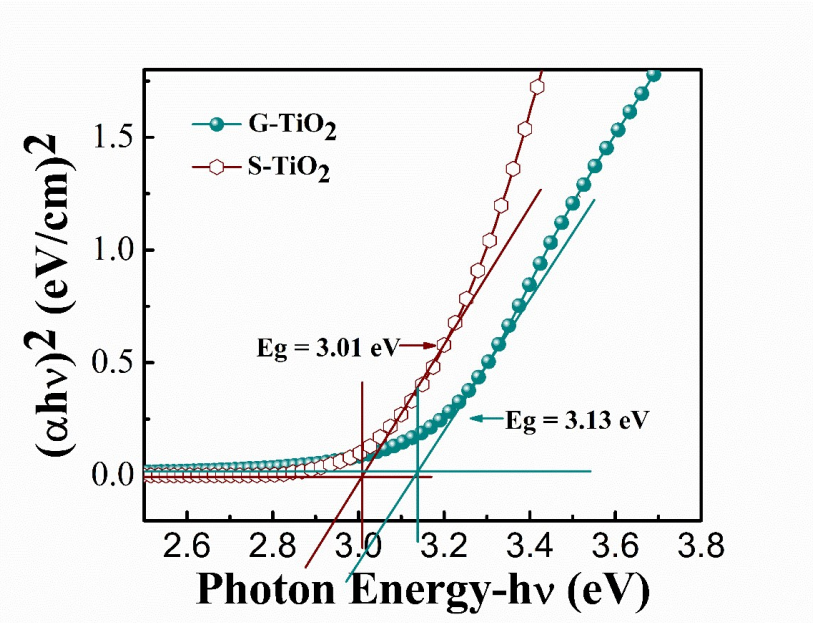

Fig. S9: Tauc plots of G-TiO_2 (dark cyan) and S-TiO_2 (burgundy).

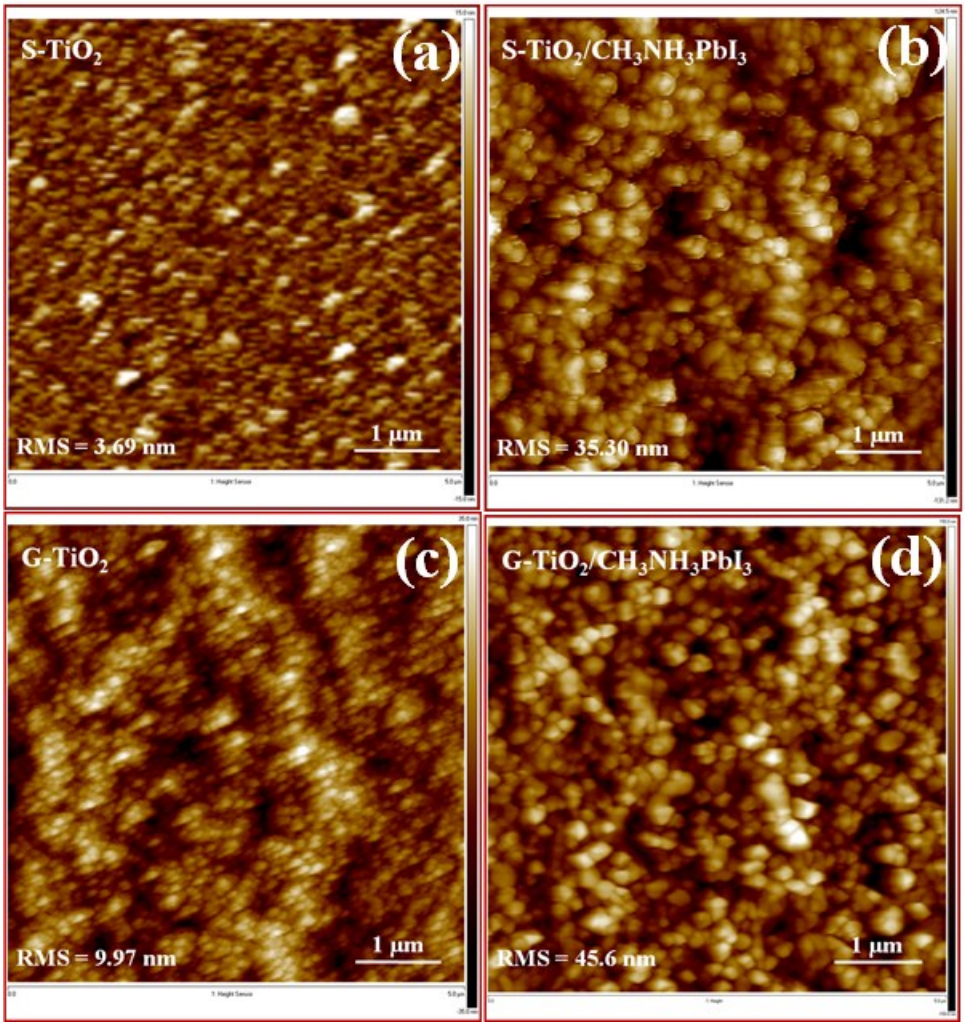

Fig. S10: AFM images of (a) glass/FTO/S-TiO_2, (b) glass/FTO/S-TiO_2/$CH_3NH_3PbI_3$, (c) glass/ITO/G-TiO_2 and (d) glass/ITO/G-TiO_2/$CH_3NH_3PbI_3$.

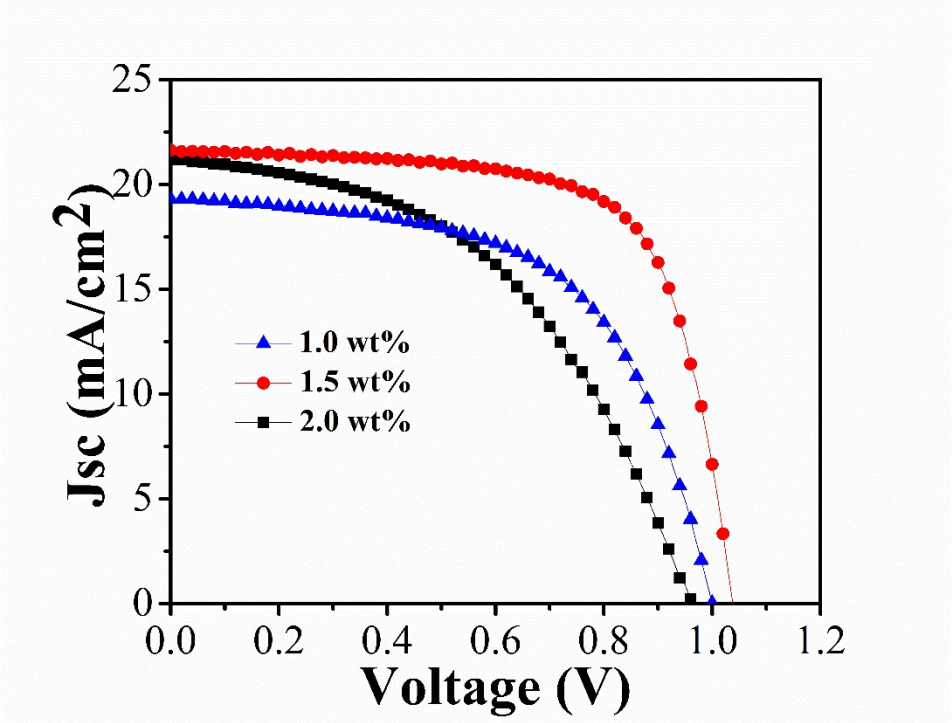

Fig. S11: *J-V* curves of PSCs based on G-TiO_2 ETL with various thicknesses prepared from different concentrations of G-TiO_2 suspension.

Reference

1 J. T.-W. Wang, J. M. Ball, E. M. Barea, A. Abate, J. A. Alexander-Webber, J. Huang, M. Saliba, I. Mora-Sero, J. Bisquert and H. J. Snaith, *Nano Lett.*, 2013, **14**, 724-730.

2 H. Zhou, Q. Chen, G. Li, S. Luo, T.-b. Song, H.-S. Duan, Z. Hong, J. You, Y. Liu and Y. Yang, *Science*, 2014, **345**, 542-546.

3 K. Wojciechowski, M. Saliba, T. Leijtens, A. Abate and H. J. Snaith, *Energy Environ. Sci.*, 2014, **7**, 1142-1147.

4 Z. Liu, Q. Chen, Z. Hong, H. Zhou, X. Xu, N. De Marco, P. Sun, Z. Zhao, Y.-B. Cheng and Y. Yang, *ACS Appl. Mater. Interfaces*, 2016, **8**, 11076-11083.

5 H. Li, W. Shi, W. Huang, E.-P. Yao, J. Han, Z. Chen, S. Liu, Y. Shen, M. Wang and Y. Yang, *Nano Lett.*, 2017, **17**, 2328-2335.

6 H. Tan, A. Jain, O. Voznyy, X. Lan, F. P. G. de Arquer, J. Z. Fan, R. Quintero-Bermudez, M. Yuan, B. Zhang and Y. Zhao, *Science*, 2017, **355**, 722-726.

7 Z. Yang, S. Zhang, L. Li and W. Chen, *J. Materiomics*, 2017.

8 W. Qiu, T. Merckx, M. Jaysankar, C. M. de la Huerta, L. Rakocevic, W. Zhang, U. Paetzold, R. Gehlhaar, L. Froyen and J. Poortmans, *Energy Environ. Sci.*, 2016, **9**, 484-489.

9 Y. Hu, S. Si, A. Mei, Y. Rong, H. Liu, X. Li and H. Han, *Solar RRL*, 2017, **1**.

10 M. Yang, Z. Li, M. O. Reese, O. G. Reid, D. H. Kim, S. Siol, T. R. Klein, Y. Yan, J. J. Berry and M. F. van Hest, *Nat. Energy*, 2017, **2**, nenergy201738.

11 A. Priyadarshi, L. J. Haur, P. Murray, D. Fu, S. Kulkarni, G. Xing, T. C. Sum, N. Mathews and S. G. Mhaisalkar, *Energy Environ. Sci.*, 2016, **9**, 3687-3692.

12 A. Agresti, S. Pescetelli, A. L. Palma, A. E. Del Rio Castillo, D. Konios, G. Kakavelakis, S. Razza, L. Cinà, E. Kymakis and F. Bonaccorso, *ACS Energy Lett.*, 2017, **2**, 279-287.

13 P. S. Shen, J. S. Chen, Y. H. Chiang, M. H. Li, T. F. Guo and P. Chen, *Adv. Mater. Interfaces*, 2016, **3**.

14 M. R. Leyden, Y. Jiang and Y. Qi, *J. Mater. Chem. A*, 2016, **4**, 13125-13132.

15 A. Fakharuddin, A. L. Palma, F. Di Giacomo, S. Casaluci, F. Matteocci, Q. Wali, M. Rauf, A. Di Carlo, T. M. Brown and R. Jose, *Nanotechnology*, 2015, **26**, 494002.

16 H. Chen, F. Ye, W. Tang, J. He, M. Yin, Y. Wang, F. Xie, E. Bi, X. Yang and M. Grätzel, *Nature*, 2017, **550**, 92-95.

17 S. Razza, F. Di Giacomo, F. Matteocci, L. Cina, A. L. Palma, S. Casaluci, P. Cameron, A. D'epifanio, S. Licoccia and A. Reale, *J. Power Sources*, 2015, **277**, 286-291.

18 M. Yang, D. H. Kim, T. Klein, Z. Li, M. O. Reese, B. Tremolet de Villers, J. Berry, M. F. van Hest and K. Zhu, *ACS Energy Lett.*, 2018.

19 P. Li, C. Liang, B. Bao, Y. Li, X. Hu, Y. Wang, Y. Zhang, F. Li, G. Shao and Y. Song, *Nano Energy*, 2018, **46**, 203-211.